Supporting Information for **Edge and 2D states disentanglement and light-driven spin injection in MoS_2**

Rodrigo Torrao[1], Syed H. Safeer[1,2], John F. R. Marroquin[3], Jorlandio F. Felix[3], Victor Carozo[4], Luiz C. Sampaio[1], and Flávio Garcia[1,*]

[1] Centro Brasileiro de Pesquisas Físicas, R. Dr. Xavier Sigaud, 150 Urca, Rio de Janeiro RJ, 22290180, Brazil.

[2] Materials Science Laboratory, Department of Physics, Quaid-i-Azam University, Islamabad, 45320, Pakistan.

[3]Departamento de Física, Pontifícia Universidade Católica do Rio de Janeiro, Rio de Janeiro, RJ 22451900, Brasil.

[4] Instituto de Física, Universidade de Brasília, Brasília, DF, 70830-200, Brazil

[*]To whom correspondence should be addressed; E-mail: fgarcia@cbpf.br

S1 MoS_2 flake quality

To support the quality of the flakes and the transfer method, several measurements were made in the as-growth flakes before transfer ($Si/SiO_2/MoS_2$) and after transfer ($GGG/YIG/MoS_2$). These measurements are addressed in this section.

S1.1 Size control

As discussed in the main manuscript, by keeping the growth conditions the same and increasing the growth time, the triangular MoS_2 flakes continue to grow in size and eventually coalesce into a uniform polycrystalline MoS_2 film [1, 2]. This behaviour can be seen in the optical images in Fig. S1(a-d), which show the MoS_2 grown at different growth times.

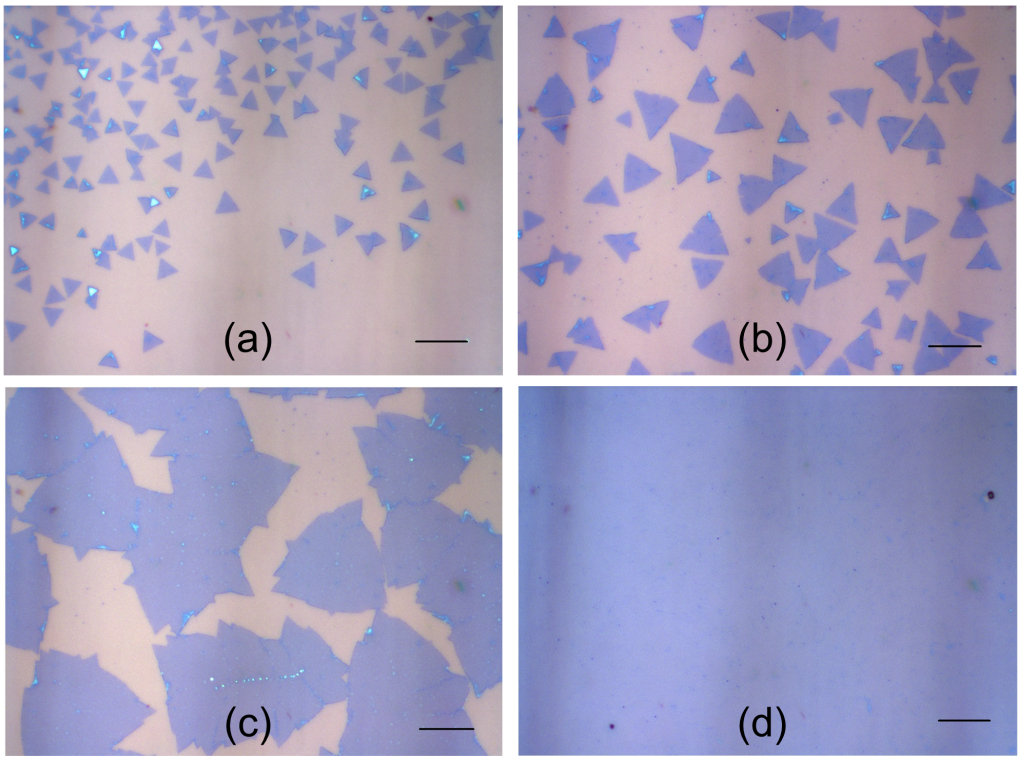

Figure S1: (a-d) Optical images showing the growth of the triangular MoS_2 monolayer into a large-area complete film. The scale bar is 20 μm.

S1.2 Optical microscopy before and after the transfer

To demonstrate the quality of the etch-free transfer method [3], Fig.S2(a) shows an optical image of a typical as-grown sample ($Si/SiO_2/MoS_2$). As can be seen, the APCVD process results in MoS_2 crystals shaped like equilateral triangles. A sulfur-rich atmosphere favors the growth of MoS_2 with

sulfur atoms at the ends, resulting in crystals with H symmetry and zigzag edges. A peculiarity of this material is that it only grows in the form of equilateral triangles when it has H symmetry and zigzag edges. This symmetry is detailed in Fig.S2(a), where the blue spheres represent molybdenum and the orange spheres represent sulfur. As shown in Fig.S2(b), the shape and morphology of the MoS_2 monolayers are preserved when transferred to the YIG (GGG/YIG/MoS_2), indicating that the transfer occurred without damage to the crystals.

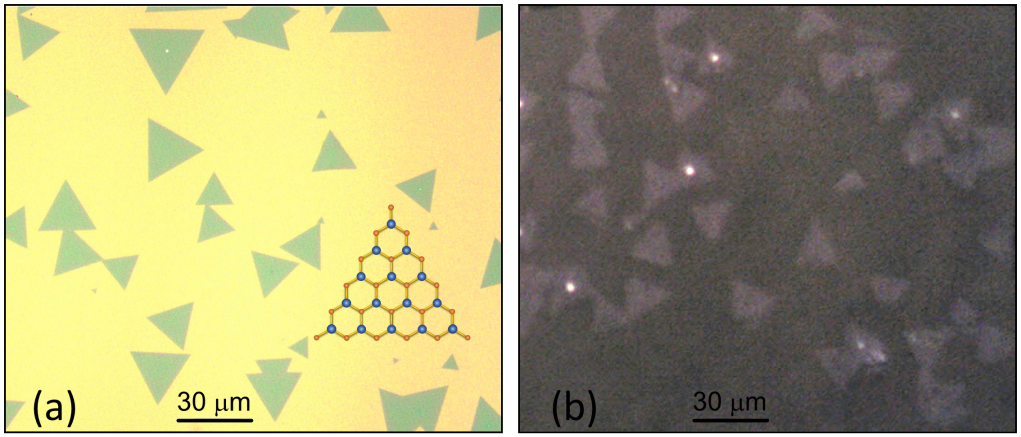

Figure S2: Optical images of the triangular MoS_2 monolayer in (a) Si/SiO_2 and (b) GGG/YIG. The scale bar is 30 μm.

S1.3 Raman spectra

To further support the quality of the flakes, the Raman spectra are shown in Fig.S3(a), for both the as-grown (red) and the transferred MoS_2 (black). As can be seen, the in-plane phonon mode E′ at 379.4 cm^{-1} and the out-of-plane mode A_1' at 399.5 cm^{-1} remained unchanged. The difference between the peak positions was 20.1 cm^{-1}, corresponding to a monolayer [4]. This result shows that the crystals were not damaged during the transfer process and did not show significant changes in lattice parameters and roughness. Also shown in Fig.S3(b) is the Raman spectrum of GGG/YIG, both before (blue) and after (red), the transfer of MoS_2 for a wider range. In the post-transfer spectrum, the in-plane and out-of-plane modes A_1' and E′ of MoS_2 are identified, along with the other peaks previously measured before the

transfer and attributed to the YIG and GGG modes. No other peaks were identified, confirming that no contamination was found after the transfer.

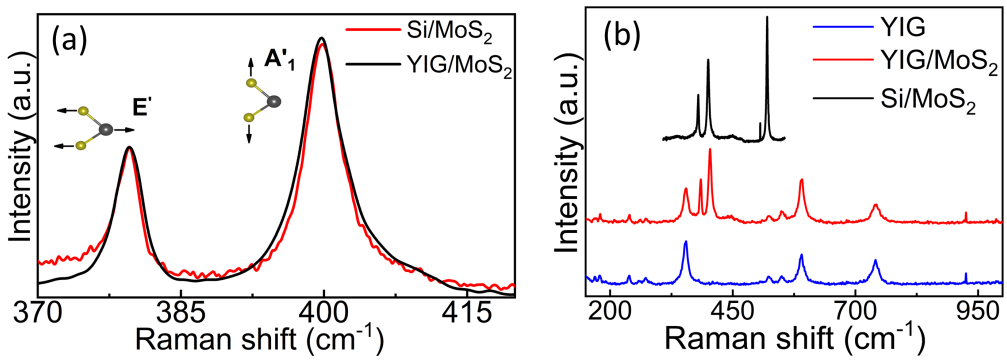

Figure S3: Normalized Raman spectra of MoS_2 flakes. In (a), GGG/YIG/MoS_2 in black and Si/SiO_2/MoS_2 in red. In (b), GGG/YIG in blue, GGG/YIG/MoS_2 in red, and Si/SiO_2/MoS_2 in black.

S1.4 Raman map

Optical microscopy showed a very low contrast for the samples transferred to the YIG compared to the microscopy performed on the samples on the silicon substrate (see Fig.S1). Raman mapping was therefore performed on some regions of the YIG/MoS_2 heterostructures. Fig. S4 shows a map of the intensity of the A_1' mode peaks for one of these crystals. Like all the measured flakes, this representative map shows a uniform intensity distribution within the triangular flakes. At the edges of the crystals, the intensity is slightly lower due to the characteristics of the beam used for mapping. This map highlights the uniformity and structural quality of the crystals, as well as their preservation after transfer.

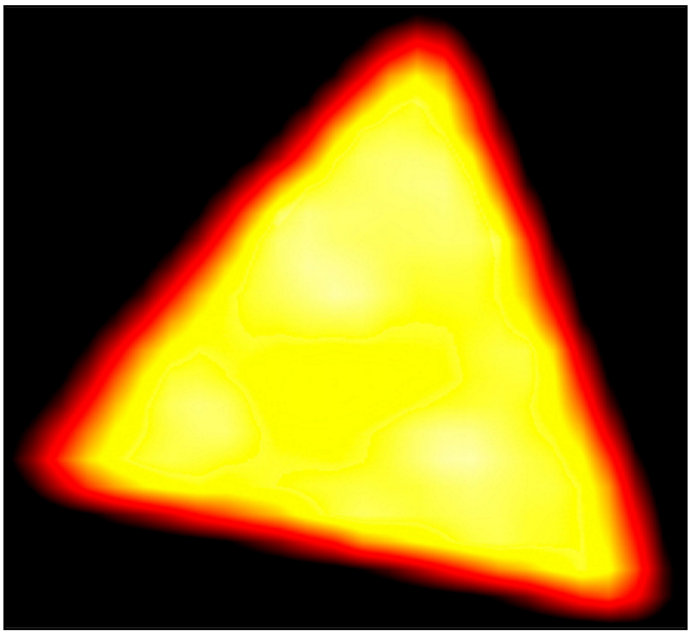

Figure S4: Raman mapping of a MoS_2 crystal, obtained from the intensity of the $A_1^{'}$ mode.

S1.5 Photoluminescence spectroscopy

The photoluminescence spectrum was recorded before and after transferring the MoS_2 flakes. In both scenarios, the observation was limited to a single neutral exciton peak located at 1.83 eV (670 nm), as shown in Fig. S5. A single and intense peak in the photoluminescence spectrum attests to the high optical quality of the MoS_2 flakes. This intense photoluminescence is associated with a direct band gap, which supports the conclusion that it is a monolayer of MoS_2, since this material in volumetric form or bilayers presents an indirect band gap.

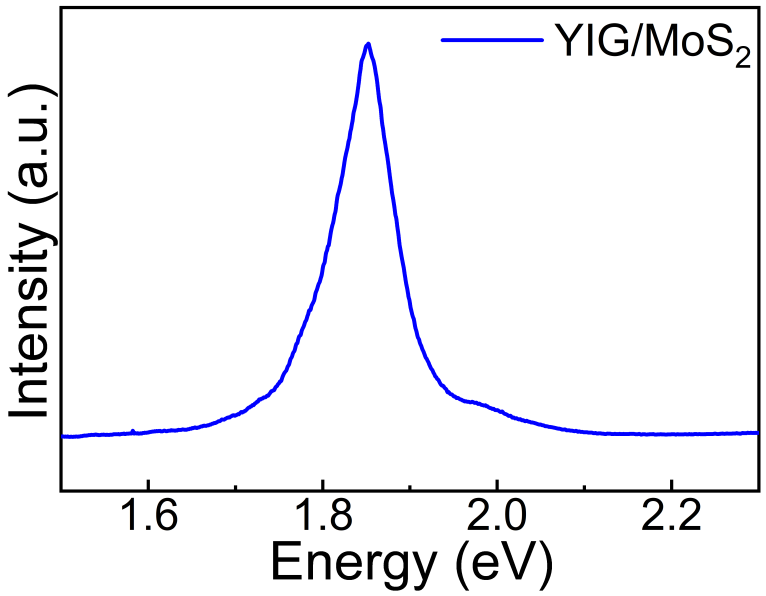

Figure S5: A photoluminescence spectrum of representative of YIG/MoS_2 heteroestructure.

S1.6 Atomic force microscopy

To further support that the flakes are monolayers, atomic force microscopy was performed on several flakes. As can be seen in Fig. S6, the difference in height of the flakes is 0.9 nm, corresponding to a MoS_2 monolayer.

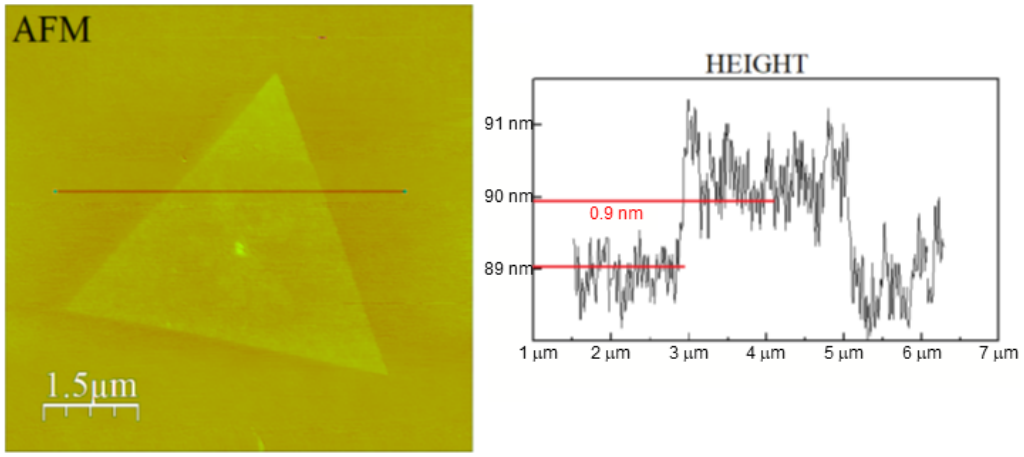

Figure S6: AFM image of a monolayer of MoS_2 triangular flake. The line profile shows a height of 0.9 nm, corresponding to a monolayer.

S2 Ferromagnetic resonance and spin pumping

The spin pumping of each sample was evaluated by the difference in the Gilbert damping of the YIG before and after the MoS_2 transfer. As described in the main manuscript, the Gilbert damping was measured using two different ferromagnetic resonance (FMR) setups [5, 6].

A fixed frequency cavity configuration with a frequency of 9.8 GHz was used for the light-exited measurements. The example of the spin pumping measurement of sample S4 is shown in Fig. S7.

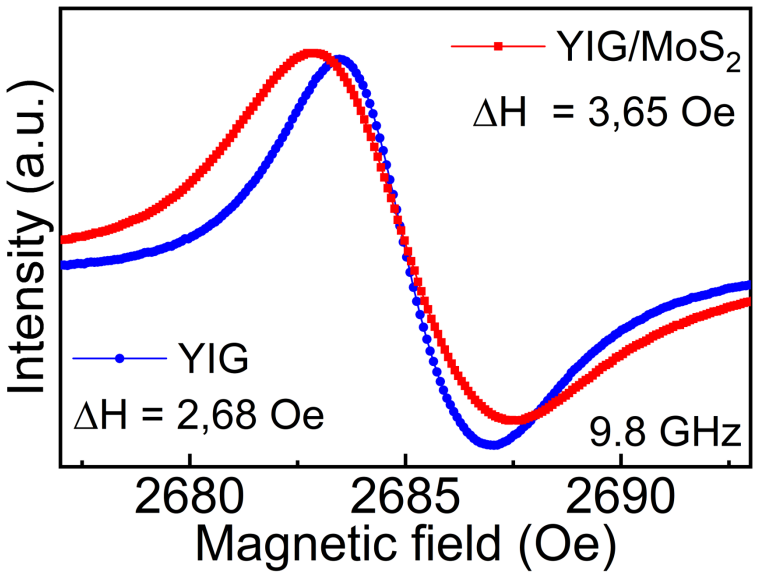

Figure S7: Ferromagnetic resonance measurement of sample S4 recorded in a fixed frequency cavity configuration at a frequency of 9.8 GHz. In blue the bare YIG and in red the YIG/MoS_2 heterostructure.

A broadband coplanar waveguide was used from 3 to 14 GHz for the FMR measurements without light incidence. The spin pumping measurements for samples S1 to S4 are shown in Fig. S8 (a) to (d).

In all cases, an AC magnetic field modulation of 0.5 Oe and 45 kHz was used for lock-in detection, and the spin pumping was evaluated using Eqs. 3 and 4 in the main manuscript.

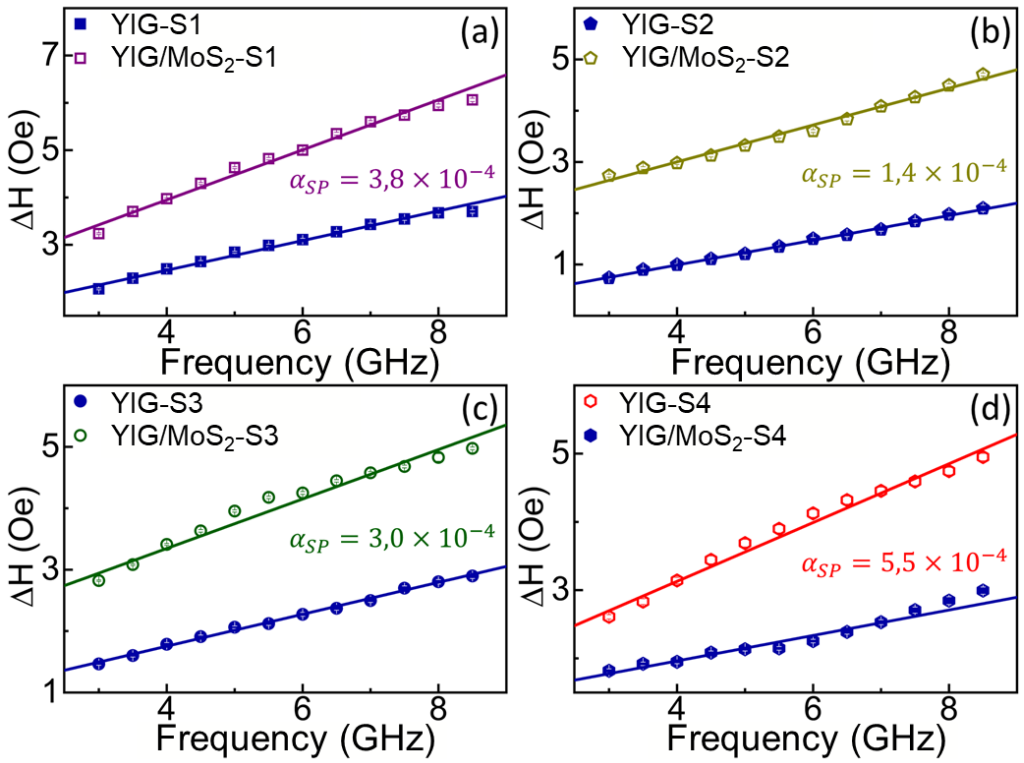

Figure S8: FMR linewidth as a function of frequency and the linear fit yields in Gilbert damping. Samples S1 to S4 are represented by the purple square (a), yellow pentagon (b), green circle (c), and red hexagon (d), respectively. The solid blue circles represent the bare YIG.

S3 FMR before and after light

The light excitation measurements were performed using three laser diodes with different wavelengths. The lasers used have a power of up to 50 mW and may have a small contribution from circular polarization. To ensure that the samples were not damaged by the light during the measurements, in Fig. S9, we show the field dependence of the derivative of the radiofrequency absorption (FMR measurements) at 9.8 GHz for samples S1 (a), S2 (b), S3 (c) and S4 (d). The solid black squares represent the measurements before any light incidence. The measurements without light incidence but after the light incidence of samples S1 to S4 are represented by the purple square (a),

yellow pentagon (b), green circle (c), and red hexagon (d), respectively. As can be seen, the measurements of the same sample before and after exposure to light are almost perfectly in agreement. This shows that the light has not damaged the MoS_2 layer and that the experimental procedure is fully reversible.

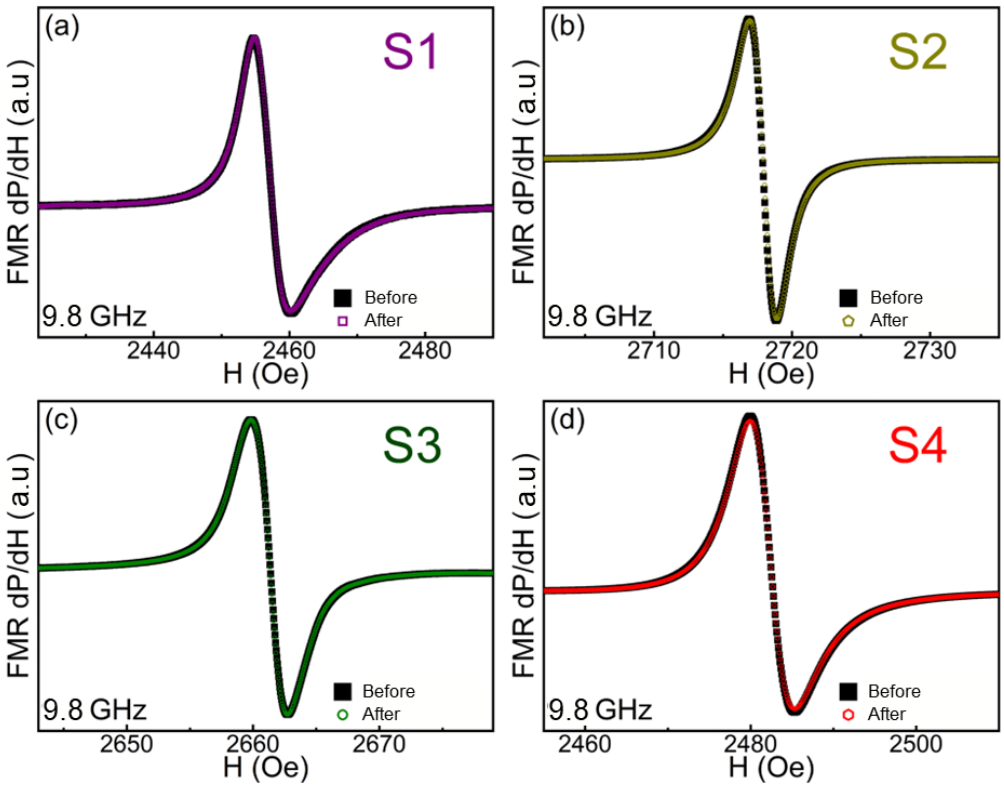

Figure S9: FMR measurements of samples S1 to S4 before (solid black squares) and after light irradiation; S1 purple square (a), S2 yellow pentagon (b), S3 green circle (c) and S4 red hexagon (d), respectively.

References

[1] Syed Hamza Safeer et al. "CVD growth and optical characterization of homo and heterobilayer TMDs". In: *Journal of Applied Physics* 132.2 (2022), p. 024301.

[2] Syed Hamza Safeer et al. “Sodium-Mediated Low-Temperature Synthesis of Monolayers of Molybdenum Disulfide for Nanoscale Optoelectronic Devices”. In: *ACS Appl. Nano Mater.* 4.4 (2021), pp. 4172–4180. ISSN: 25740970. DOI: 10.1021/acsanm.1c00491.

[3] Syed Hamza Safeer et al. “Etching-Free Transfer and Nanoimaging of CVD-Grown MoS2 Monolayers”. In: *The Journal of Physical Chemistry C* 125.38 (2021), pp. 21011–21017.

[4] Yi-Hsien Lee et al. “Synthesis of large-area MoS2 atomic layers with chemical vapor deposition”. In: *Advanced materials* 24.17 (2012), pp. 2320–2325.

[5] R Torrão et al. “Reproducible low Gilbert damping yttrium iron garnet by magnetron sputtering”. In: *Journal of Alloys and Compounds* 923 (2022), p. 166300.

[6] Rodrigo Torrão Victor et al. “Automated mechanical exfoliation technique: a spin pumping study in YIG/TMD heterostructures”. In: *Nanoscale Horizons* 8.11 (2023), pp. 1568–1576.